

Phase Transformations of the Ternary System $(\text{NH}_4)_2\text{SO}_4$ - H_2SO_4 - H_2O and the Implications for Cirrus Cloud Formation

Scot T. Martin

Department of Environmental Sciences and Engineering, The University of North Carolina at Chapel Hill, Chapel Hill, NC 27599-7400, USA

Abstract. Homogeneous and heterogeneous growth mechanisms for cirrus cloud formation are considered in light of recent measurements showing the presence of NH_4^+ ions in the aerosol of the upper troposphere. Low-temperature ternary phase diagrams of $(\text{NH}_4)_2\text{SO}_4$ - H_2SO_4 - H_2O are presented, and the thermodynamic and the kinetic data of the phase transitions are employed to consider the implications of NH_4^+ ions on the mechanisms of cirrus cloud formation. The analysis concludes that changes in the degree of ammoniation can lead to a crossover in the cloud growth system from homogeneous to heterogeneous nucleation. A corresponding change in the cloud's particle distribution alters the cloud's radiative properties, persistence, and surface area available for heterogeneous chemistry.

Introduction

The largest single uncertainty in quantitative models of global warming is the contribution by clouds [IPCC, 1996]. Clouds play the countervailing roles of absorbing near infrared radiation, which insulates or warms Earth, and scattering the sun's visible radiation upward, thus cooling Earth. In addition, clouds strongly influence the climate system via the hydrologic cycle and heterogeneous chemistry. The highest altitude clouds from 70°S to 70°N are cirrus clouds, and their formation is of considerable current interest. Cirrus clouds are typically composed of ice particles formed in the upper troposphere (UT), in which atmospheric conditions range from -30 to -70°C and the partial pressure of water rarely exceeds a saturation ratio of 1.5 with respect to the vapor pressure of ice.

A cirrus cloud is believed to form during the cooling of an air mass containing hygroscopic particles [Jensen and Toon, 1994a]. The particles uptake water, become metastable with respect to ice, and then nucleate ice to begin the cloud formation process. Ice nucleation can occur either by homogeneous freezing of supercooled droplets or by heterogeneous freezing in droplets containing soot or crustal components.

Until recently, the predominant aerosol measured in the UT was composed of aqueous H_2SO_4 [Sheridan *et al.*, 1994] and insoluble constituents [Hagen *et al.*, 1994]. In April and May 1996, airborne measurements of UT particles over the continental United States were made as part of the *Subsonic aircraft: Contrail and Cloud Effects Special Study* mission. Those measurements revealed the occurrence of NH_4^+ in UT particles. Particle compositions are then ternary mixtures of $(\text{NH}_4)_2\text{SO}_4$ - H_2SO_4 - H_2O . The unknown extent of partially neutralized UT aerosols on a global scale notwithstanding, how do NH_4^+ ions affect the rate of ice nucleation and the subsequent formation of cirrus clouds? This paper addresses that question by employing thermodynamic and kinetic data of the phase transitions of $(\text{NH}_4)_2\text{SO}_4$ - H_2SO_4 - H_2O .

Phase Diagrams

The phase diagram of $(\text{NH}_4)_2\text{SO}_4\text{-H}_2\text{SO}_4\text{-H}_2\text{O}$ at 298 K is shown in Fig. 1 and is calculated from the model of Clegg and Brimblecombe [1995]. To include the effects of temperature, a three-dimensional phase diagram is constructed conceptually by stacking isothermal sheets on top of one another. From this three-dimensional diagram, temperature-dependent transects are made along the x-axis, the line $m = 1.375$ (viz. stoichiometric NH_4HSO_4), and the y-axis to generate Figs. 2A-C. Fig. 2A shows the $\text{H}_2\text{SO}_4\text{-H}_2\text{O}$ binary phase diagram. The relative humidity (RH) contours are calculated from the model of Carslaw et al. [1995] and the parameterization of Tabazadeh et al. [1997] above and below 260 K, respectively.

The phase-diagrams of $\text{NH}_4\text{HSO}_4\text{-H}_2\text{O}$ and $(\text{NH}_4)_2\text{SO}_4\text{-H}_2\text{O}$ are shown in Figs. 2B and C, respectively. Low-temperature thermodynamic data for these systems are limited, so the Clausius-Clapeyron equation is employed to extrapolate to lower temperatures. As such, Figs. 2B and C should be considered qualitatively instructive rather than quantitatively accurate. $P_{\text{H}_2\text{O}}(\text{wt}\%, 298\text{K})$ [Tang and Munkelwitz, 1994] and $P_{\text{H}_2\text{O,ice}}(T)$ at the freezing point temperature [Imre et al., 1997; Seidell, 1940; Weast et al., 1983] are employed to calculate $\Delta H_{\text{vap}}(\text{wt}\%)$ through re-arrangement of the Clausius-Clapeyron equation, as follows:

$$\Delta H_{\text{vap}}(\text{wt}\%) = R \left(\frac{1}{298} - \frac{1}{T_{\text{ice depression}}} \right)^{-1} \ln \frac{P_{\text{H}_2\text{O}}(\text{wt}\%, 298\text{K})}{P_{\text{H}_2\text{O}}(\text{wt}\%, T_{\text{ice depression}})} \quad (1)$$

Values of ΔH_{vap} beyond the eutectic composition are obtained by linear extrapolation. In this way, ΔH_{vap} is estimated as a function of composition. The ΔH_{vap} values are employed to calculate $P_{\text{H}_2\text{O}}(\text{wt}\%, T)/P_{\text{H}_2\text{O}}(\text{water}, T)$ at low temperatures through re-arrangement of eq 1. Although this estimation procedure is necessary based upon the limitations of available data, there are several shortcomings. Foremost, ΔH_{vap} is not temperature-independent, but rather it varies with heat capacity according to Kirchhoff's Law. For example, ΔH_{vap} of water increases by 1% for every 10 K in cooling. The polynomial coefficients parameterizing the relative humidity values are provided in Table 1.

The temperature dependent solubilities shown in Figs. 2B and C for the solids $(\text{NH}_4)_2\text{SO}_4$ [Wexler and Seinfeld, 1991], NH_4HSO_4 [Imre et al., 1997], ice [Imre et al., 1997; Seidell, 1940], and $\text{NH}_4\text{HSO}_4 \cdot 8\text{H}_2\text{O}$ [Imre et al., 1997] are obtained from literature. Below the eutectic composition, the ice line follows an ice saturation rate, S_{ice} , of unity, which is calculated by employing $P_{\text{H}_2\text{O,ice}}(T)$ from Carslaw et al. [1995]. Comparison of literature RH values along the liquidus lines of $(\text{NH}_4)_2\text{SO}_4$, NH_4HSO_4 , and $\text{NH}_4\text{HSO}_4 \cdot 8\text{H}_2\text{O}$ to the RH contours calculated in Figs. 2B and C can be employed as a measure of accuracy of the procedure discussed for eq 1. According to Fig. 2C, $(\text{NH}_4)_2\text{SO}_4$ is in equilibrium with 44 wt% solution at 78% RH at 298 K, compared to measured values of 79-80% RH. Similarly, there is good agreement for NH_4HSO_4 in equilibrium at 298 K (i.e., 40% RH from Fig. 2B and 40% measured). At the peritectic transition of NH_4HSO_4 and $\text{NH}_4\text{HSO}_4 \cdot 8\text{H}_2\text{O}$, the RH is 60% according to Fig. 2B and has been measured as 64.5%. At the eutectic of ice and $\text{NH}_4\text{HSO}_4 \cdot 8\text{H}_2\text{O}$, the calculated and measured RH values are 72 and 70%, respectively.

Atmospheric Implications

Phase transitions are chemical reactions involving complex kinetics, for which the nucleation rate of a critical embryo is often the rate-limiting step. For common atmospheric

processes, deliquescence and melting are kinetically fast and thus particle composition along atmospheric trajectories of decreasing temperature show no deviation from the phase diagram. Efflorescence and freezing, on the other hand, are usually kinetically hindered because a free energy barrier must be overcome to form an ordered germ. Aqueous $(\text{NH}_4)_2\text{SO}_4$ droplets, for example, do not homogeneously effloresce until 40% RH at 298 K. The critical water activity saturation ratio, S^* , is 2.0 at efflorescence. Water droplets similarly supercool by 40 K before homogeneous ice nucleation occurs, at which point $S^* = 1.47$. Aqueous droplets of NH_4HSO_4 as well as H_2SO_4 also supercool by 40 K before ice nucleation begins [Imre *et al.*, 1997]; in the absence of experimental data, aqueous $(\text{NH}_4)_2\text{SO}_4$ droplets are assumed to supercool also by 40 K. Past the peritectic composition, concentrated aqueous droplets of NH_4HSO_4 supercool by 40 K [Imre *et al.*, 1997].

Knowledge of kinetic deviations from the phase diagrams along atmospheric trajectories of decreasing temperature is important because ice crystallization is the key initiation step in cirrus cloud formation. Trajectories of decreasing temperature are shown in Figs. 2A-C at constant H_2O partial pressures, corresponding to ice frost points of -40, -55, and -70°C. These trajectories follow within several percent the expansion at constant potential temperature of a rising air parcel. The trajectories would be modified when particle size or mass transfer is important.

Consider the trajectories T_{11} , T_{12} , and T_{13} in Figs 2A-C. In Fig 2A, hygroscopic aqueous H_2SO_4 particles uptake water, with a doubling in volume, between 260 and 229.73 K along T_{11} . Because the radius and optical constants of the particle change, there are minor associated changes in radiative forcing. At 229.73 K (7.6 wt%), ice formation is initiated by homogeneous nucleation, and numerous small ice particles form a cirrus cloud. The freezing temperature is obtained when the temperature difference between T_{11} line and the ice line (d) in Fig. 2A equals 40. For NH_4HSO_4 along T_{12} , when the initial RH along the trajectory is above 35%, particles probably begin as liquid because concentrated aqueous NH_4HSO_4 supercools by 40 K with respect to crystalline NH_4HSO_4 . In this case, the particles undergo hygroscopic growth until ice nucleation begins at 229.64 (9.1 wt%), as given by 40 K supercooling between the T_{12} line and the ice line (d) in Fig. 2B. For $(\text{NH}_4)_2\text{SO}_4$ along T_{13} , the particles may be either liquid or solid at the start of the trajectory because it is not known to what extent concentrated aqueous $(\text{NH}_4)_2\text{SO}_4$ supercools with respect to crystalline $(\text{NH}_4)_2\text{SO}_4$. At 298 K, there is a 40% RH hysteresis between deliquescence and efflorescence. If this result is adopted as a principle to apply at lower temperatures, then T_{13} is either a liquid or solid whereas T_{23} and T_{33} are solids at the beginning of the trajectory. A liquid along T_{13} is hygroscopic until 229.54 K (12.7 wt%), at which point supercooling of 40 K is obtained and homogeneous ice nucleation takes place. A solid along T_{13} , however, does not take up water and there is no change in particle size until deliquescence at 230.81 K (37.9 wt%), which is followed by hygroscopic growth and freezing at 229.54 K. Based upon this kinetic analysis of trajectories in the phase diagrams shown in Figs. 2A-C, the activation temperature for cirrus cloud nucleation changes from 229.73 to 229.54 K as the solution composition shifts from acidic to neutral.

The kinetic analysis can be extended to lower temperatures along trajectories T_{2x} . Hygroscopic H_2SO_4 particles along T_{21} behave similarly to those along T_{11} , and freezing occurs at

215.36 K (22.7 wt%). SAT, indicated by the solubility line *f* in Fig. 2A, does not form readily. Along T_{22} , particles begin as solid NH_4HSO_4 (deeper than 40 K supercooling), deliquesce at 217.15 K (24.9 wt%), grow hygroscopically, and freeze to form ice at 216.03 K (18.9 wt%). Trajectory T_{23} is deceptively similar. The particles begin as solid $(\text{NH}_4)_2\text{SO}_4$ and deliquesce at 214.81 K (36.7 wt%). The liquid particles are supercooled by 42.1 K with respect to ice and thus immediately form ice. If deliquescence were not necessary, then ice formation would initiate at 214.93 K (39.5 wt%). However, because deliquescence is necessary, the solid thus further depresses the critical temperature for cirrus cloud formation to begin.

Trajectories T_{3x} are along the lowest temperatures and $P_{\text{H}_2\text{O}}$ conditions commonly found in the UT. Similar to T_{11} and T_{21} , hygroscopic H_2SO_4 particles nucleate neither SAT nor SAH, and ice nucleation begins at 201.01 (29.1 wt%) along T_{31} in Fig. 2A. Trajectory T_{32} is similar to T_{23} because solid NH_4HSO_4 deliquesce and freeze immediately (60.2 K supercooling) at 200.24 K (16.4 wt%), as compared to 202.03 K (25.1 wt%) for 40 K supercooling with respect to ice. Solid $(\text{NH}_4)_2\text{SO}_4$ along T_{33} deliquesces and freezes at 199.27 K (35.6 wt%), supercooled with respect to ice by 58.4 K. Because $S_{\text{ice}} = 1.80$ at that point, it is also possible that direct vapor deposition of ice onto solid $(\text{NH}_4)_2\text{SO}_4$ occurs at higher temperatures where S_{ice} is between 1.5 and 1.7, corresponding to 200.46 to 199.65 K.

Along T_{1y} , T_{2y} , and T_{3y} , the activation temperatures range among 229.5-229.7, 214.8-216.0, and 199.3-201.0 K, respectively. Considered by themselves, these small ranges do not alter cirrus cloud formation significantly. The altitude for activation shifts upwards by 250 m, and there are changes in the evolution of optical properties and surface area prior to activation. However, in addition to the homogeneous freezing mechanisms considered thus far, cirrus cloud formation also arises from heterogeneous freezing on a variety of insoluble constituents, believed largely to be particulates of Earth's crustal components. In an air parcel, there are a relatively large number of particles potentially susceptible to homogeneous freezing. When this mode is active, a cloud forms with numerous but small ice particles. Conversely, there are relatively few numbers of heterogeneous nuclei so that a cloud with few, large ice particles forms when this mode is active. The dominant mode depends on several factors, including the particle concentration, the concentration of heterogeneous nuclei, the rate of cooling, and the relative humidity [Jensen *et al.*, 1994b]. Atmospheric measurements show that the concentration of activated heterogeneous nuclei is often given by $N_{\text{IN}} = CS_{\text{ice}}^k$ where N_{IN} is the concentration of ice nuclei (IN), C is a concentration scaling variable specific to an air parcel, and k is a constant within an air parcel varying with the nature of IN present [Pruppacher and Klett, 1978]. The temperature ranges noted above correspond to S_{ice}^* shifted from 1.48 to 1.51, from 1.31 to 1.55, and from 1.38 to 1.80, respectively. The increased supersaturations permit an additional ΔN heterogeneous nuclei to activate. For example, setting $k = 5$, which is a median value of actual observations, N_{IN} increases by 400% as S_{ice} increases from 1.38 to 1.80. At an upper limit of $k = 10$, N_{IN} increases 1,400%. Although calculations of the dominant formation mechanisms require consideration of other case specific factors (*vide supra*), increasing concentrations of heterogeneous nuclei favor the formation of a cirrus cloud with few, large ice particles.

Numerical simulations of cirrus cloud formation have been carried out based upon the deliquescence of $(\text{NH}_4)_2\text{SO}_4$ [DeMott et al., 1994; Heymsfield and Sabin, 1989; Jensen et al., 1994a; Sassen and Dodd, 1989] and the hygroscopic uptake by H_2SO_4 [Jensen et al., 1994b]. A full microphysical model of cloud formation considered the important factors balancing the rates of homogeneous and heterogeneous processes and thus the mode of cirrus cloud formation for a *fixed aerosol composition* of either $(\text{NH}_4)_2\text{SO}_4$ or H_2SO_4 [Jensen et al., 1994a]. The present paper points out that a *variable aerosol composition* implies a shift in the cross-over conditions from a homogeneous to a heterogeneous mode.

The contributions of heterogeneous versus homogeneous freezing processes to cirrus cloud formation and the effects of the particle composition, either as H_2SO_4 or $(\text{NH}_4)_2\text{SO}_4$, are evaluated by DeMott et al. [1997]. The authors conclude that heterogeneous nuclei lead to the largest changes in ice particle density, when compared to purely homogeneous nucleation, at higher temperatures and more acidic compositions. The present paper concludes that the activity of heterogeneous nuclei increases with neutralization and colder temperatures. The contradiction between the conclusions is rooted in the assumptions made concerning heterogeneous nucleation. DeMott et al. assume that aqueous $(\text{NH}_4)_2\text{SO}_4$ supercools more deeply with respect to ice than H_2SO_4 does, that heterogeneous nucleation of ice from aqueous $(\text{NH}_4)_2\text{SO}_4$ is thus slower than from H_2SO_4 at the same temperature, and that heterogeneous ice nucleation on soot particles provides a representative lower limit for tropospheric particles. The related assumptions in this paper are that aqueous $(\text{NH}_4)_2\text{SO}_4$ supercools by 40 K, in analogy to H_2SO_4 and NH_4HSO_4 , and that the efficiency of heterogeneous nucleation is a function of water activity (i.e., S_{ice}), given by $N_{\text{IN}} = CS_{\text{ice}}^k$, regardless of solution composition. Resolution of the accuracy of these assumptions requires further experimental evidence. In a second difference, DeMott et al. employ parameterizations of hygroscopicity at 298 K to low temperature water uptake. In this paper the low-temperature differences in hygroscopicity, as shown in Figs. 2A-C, are employed. The slope of the RH lines, especially in Fig. 2B, show that the low-temperature variation in hygroscopicity can be significant. Despite these differences, the common message of DeMott et al. and this paper is that the extent of neutralization of $(\text{NH}_4)_2\text{SO}_4$ - H_2SO_4 - H_2O particles affects cirrus cloud formation primarily via effects on heterogeneous nucleation.

Several final caveats should be mentioned. Atmospheric particles are likely partially neutralized, consisting of nonstoichiometric compositions ($0 < x < 2$) of $(\text{NH}_4)_x\text{H}_{2-x}\text{SO}_4$. This paper analyzes the poles ($x = 0$ and 2) and the mid-point ($x = 1$). Conclusions on intermediate neutralizations are based upon interpolation. Future experimental results may reveal that interpolation is not appropriate, especially near $x = 1.5$ in the vicinity of letovicite. Along T_{x2} , particles are metastable to $\text{NH}_4\text{HSO}_4 \cdot 8\text{H}_2\text{O}$. In the absence of further experimental information on this solid and other possible low temperature solids (e.g., nucleation of letovicite), these possible phase transitions are omitted from the present analysis.

Conclusions

Increasing neutralization and decreasing temperatures affect ice formation from $(\text{NH}_4)_2\text{SO}_4$ - H_2SO_4 - H_2O particles by shifting S_{ice}^* for homogeneous nucleation upwards. For example,

complete neutralization shifts S_{ice}^* from 1.38 to 1.80 at -70°C . As $S_{ice,homogeneous}^*$ increases and homogeneous nucleation is thus inhibited, the predominance of heterogeneous nucleation may increase. Changes in the degree of ammoniation can thus lead to a crossover in the cloud growth system from homogeneous to heterogeneous mode nucleation, and a corresponding change in the cloud's particle distribution from many small particles to relatively few large particles. The change in the cloud alters its radiative properties, precipitation, lifetime, and surface area for heterogeneous chemistry.

Although the existing thermodynamic and kinetic information on low temperature phase transitions of ternary $(\text{NH}_4)_2\text{SO}_4\text{-H}_2\text{SO}_4\text{-H}_2\text{O}$ system is incomplete, it has been valuable at this juncture to provide a perspective on the implications for NH_4^+ incorporated into UT particles.

Acknowledgments. Paul J. DeMott provided valuable comments. The Petroleum Research Fund, administered by the American Chemical Society (ACS-PRF# 32580-G9), provided financial support.

References

- Carslaw, K.S., S.L. Clegg, and P. Brimblecombe, A Thermodynamic Model of the System $\text{HCl-HNO}_3\text{-H}_2\text{SO}_4\text{-H}_2\text{O}$, Including Solubilities of HBr , from <200 to 328 K, *J. Phys. Chem.*, *99*, 11557-11574, 1995.
- Clegg, S.L., and P. Brimblecombe, A generalised multicomponent thermodynamic model applied to the $(\text{NH}_4)_2\text{SO}_4\text{-H}_2\text{SO}_4\text{-H}_2\text{O}$ system to High supersaturation and low relative humidity at 298.15 K, *J. Aerosol Sci.*, *26*, 19-38, 1995.
- DeMott, P.J., M.P. Meyers, and W.R. Cotton, Parameterization and impact of ice initiation processes relevant to numerical model simulations of cirrus clouds, *J. Atmos. Sci.*, *51*, 77-90, 1994.
- DeMott, P.J., D.C. Rogers, and S.M. Kreidenweis, The susceptibility of ice formation in upper tropospheric clouds to insoluble aerosol components, *J. Geophys. Res.*, *102*, 19575-19584, 1997.
- Hagen, D.E., et al., Potential role of nuclei in cloud element formation at high altitudes, *Atmos. Res.*, *31*, 123-135, 1994.
- Heymsfield, A.J., and R.M. Sabin, Cirrus crystal nucleation by homogeneous freezing of solution droplets, *J. Atmos. Sci.*, *46*, 2252-2264, 1989.
- Imre, D.G., J. Xu, and R. McGraw, Ammonium bisulfate/water equilibrium and metastability phase diagrams, *J. Phys. Chem.*, *101*, 4191, 1997.
- IPCC, The Science of Climate Change, in *Climate Change* 1995, Cambridge University Press, New York, 1996.
- Jensen, E.J., O.B. Toon, D.L. Westphal, S. Kinne, and A.J. Heymsfield, Microphysical modeling of cirrus. 1. Comparison with 1986 FIRE IFO measurements, *J. Geophys. Res.*, *99*, 10421-10442, 1994a.
- Jensen, E.J., and O.B. Toon, Ice nucleation in the upper troposphere: Sensitivity to aerosol number density, temperature, and cooling rate, *Geophys. Res. Letts.*, *21*, 2019-2022, 1994b.
- Pruppacher, H.R., and J.D. Klett, *Microphysics of Clouds and Precipitation*, Kluwer Academic Publishers, Dordrecht, Holland, 1997.
- Sassen, K., and G.C. Dodd, Haze particle nucleation simulations in cirrus clouds, and applications for numerical and lidar studies, *J. Atmos. Sci.*, *46*, 3005-3014, 1989.
- Seidell, A., *Solubilities of Inorganic and Metal Organic Compounds*, Nostrand, New York, 1940.
- Sheridan, P.J., C.A. Brock, and J.C. Wilson, Aerosol particles in the upper troposphere and lower stratosphere, *Geophys. Res. Letts.*, *21*, 2587-2590, 1994.
- Tabazadeh, A., O.B. Toon, S.L. Clegg, and P. Hamill, A new parameterization of $\text{H}_2\text{SO}_4/\text{H}_2\text{O}$ aerosol composition: Atmospheric implications, *Geophys. Res. Lett.*, *24*, 1931-1934, 1997.
- Tang, I.N., and H.R. Munkelwitz, Water activities, densities, and refractive indices of aqueous sulfates and sodium nitrate droplets of atmospheric importance, *J. Geophys. Res.*, *99*, 18801-18808, 1994.
- Wexler, A.S., and J.H. Seinfeld, Second-Generation Inorganic Aerosol Model, *Atmos. Environ.*, *25A*, 2731-2748, 1991.

(Received: November 21, 1997; revised: February 5, 1998; accepted: February 16, 1998)

Table 1. Coefficients for the parameterization of the relative humidity values of aqueous solutions of $(\text{NH}_4)_2\text{SO}_4$ and NH_4HSO_4 . At the temperatures indicated, $RH = \sum_i c_i w^i$ where w is the weight percent composition.

$(\text{NH}_4)_2\text{SO}_4$		Coefficient				
T (K)	c_0	$10^3 c_1$	$10^4 c_2$	$10^6 c_3$	$10^8 c_4$	$10^{10} c_5$
200	1.0000	2.6474	-5.7114	18.9684	-	12.5361
210	0.9999	1.7912	-4.7935	15.7719	-	10.6872
220	0.9999	1.0150	-3.9605	12.8650	-	8.9952
230	0.9999	0.3083	-3.2012	10.2105	-	7.4416
240	0.9998	-0.3378	-2.5062	7.7773	-	6.0103
250	0.9998	-0.9308	-1.8679	5.5392	-9.0373	4.6878
260	0.9998	-1.4769	-1.2795	3.4737	-6.3108	3.4625
270	0.9997	-1.9814	-0.7356	1.5619	-3.7825	2.3241
280	0.9997	-2.4489	-0.2312	-0.2127	-1.4317	1.2640
290	0.9997	-2.8833	0.2378	-1.8643	0.7593	0.2743
300	0.9996	-3.2880	0.6749	-3.4051	2.8063	-0.6516

NH_4HSO_4		Coefficient					
T (K)	c_0	$10^3 c_1$	$10^4 c_2$	$10^5 c_3$	$10^7 c_4$	$10^9 c_5$	$10^{11} c_6$
200	1.0029	21.4095	-	19.0353	-	37.0466	-
210	1.0023	18.1379	-	16.3358	-	31.6677	-
220	1.0018	15.0854	-	13.8628	-	26.7824	-9.9605
230	1.0014	12.2322	-	11.5906	-	22.3281	-8.2953
240	1.0011	9.5603	-	9.4967	-	18.2517	-6.7741
250	1.0008	7.0538	-	7.5619	-	14.5083	-5.3794
260	1.0005	4.6985	-	5.7694	-	11.0595	-4.0965
270	1.0003	2.4816	-	4.1047	-8.2194	7.8727	-2.9129
280	1.0002	0.3917	-6.4393	2.5549	-5.1421	4.9195	-1.8177
290	1.0000	-1.5815	-3.0144	1.1089	-2.2790	2.1757	-0.8017
300	0.9999	-3.4473	0.2092	-0.2431	0.3911	-0.3799	0.1431

Figure Captions

Figure 1. Phase diagram of $(\text{NH}_4)_2\text{SO}_4\text{-H}_2\text{SO}_4\text{-H}_2\text{O}$ at 298 K. Relative humidity contours for the liquid are shown by the dashed lines. The solubilities of the solid phases $(\text{NH}_4)_2\text{SO}_4$ (a), $(\text{NH}_4)_3\text{H}(\text{SO}_4)_2$ (b), and NH_4HSO_4 (c) are indicated by the solid lines. The liquid solution is metastable in regions exceeding the solubilities of the solid phases.

Figure 2. Temperature-dependent phase diagrams along transects of Fig. 1. Relative humidity contours for the liquid are shown by the thin dashed lines. The solubilities of the solid phases $(\text{NH}_4)_2\text{SO}_4$ (a), $(\text{NH}_4)_3\text{H}(\text{SO}_4)_2$ (b), NH_4HSO_4 (c), ice (d), $\text{H}_2\text{SO}_4\cdot 6.5\text{H}_2\text{O}$ (e), $\text{H}_2\text{SO}_4\cdot 4\text{H}_2\text{O}$ (f), and $\text{NH}_4\text{HSO}_4\cdot 8\text{H}_2\text{O}$ (g) are indicated by the solid lines. The liquid solution is metastable in regions exceeding the solubilities of the solid phases. Thick dashed lines show the liquidus lines of solids in regions where the liquid is supercooled with respect to another solid. Temperature trajectories, T_{xy} , are shown along lines of constant H_2O partial pressure with respect to the liquid phase, where x denotes the ice-frost point temperature as -40 (1), -55 (2), or -70°C (3) and y denotes the transect as H_2SO_4 (1), NH_4HSO_4 (2), or $(\text{NH}_4)_2\text{SO}_4$ (3). (A) H_2SO_4 temperature transect along the x-axis in Fig. 1. (B) NH_4HSO_4 temperature transect along $m = 1.375$ in Fig. 1. (C) $(\text{NH}_4)_2\text{SO}_4$ temperature transect along the y-axis in Fig. 1.

Figure 1. Phase diagram of $(\text{NH}_4)_2\text{SO}_4\text{-H}_2\text{SO}_4\text{-H}_2\text{O}$ at 298 K. Relative humidity contours for the liquid are shown by the dashed lines. The solubilities of the solid phases $(\text{NH}_4)_2\text{SO}_4$ (a), $(\text{NH}_4)_3\text{H}(\text{SO}_4)_2$ (b), and NH_4HSO_4 (c) are indicated by the solid lines. The liquid solution is metastable in regions exceeding the solubilities of the solid phases.

Figure 2. Temperature-dependent phase diagrams along transects of Fig. 1. Relative humidity contours for the liquid are shown by the thin dashed lines. The solubilities of the solid phases $(\text{NH}_4)_2\text{SO}_4$ (a), $(\text{NH}_4)_3\text{H}(\text{SO}_4)_2$ (b), NH_4HSO_4 (c), ice (d), $\text{H}_2\text{SO}_4\cdot 6.5\text{H}_2\text{O}$ (e), $\text{H}_2\text{SO}_4\cdot 4\text{H}_2\text{O}$ (f), and $\text{NH}_4\text{HSO}_4\cdot 8\text{H}_2\text{O}$ (g) are indicated by the solid lines. The liquid solution is metastable in regions exceeding the solubilities of the solid phases. Thick dashed lines show the liquidus lines of solids in regions where the liquid is supercooled with respect to another solid. Temperature trajectories, T_{xy} , are shown along lines of constant H_2O partial pressure with respect to the liquid phase, where x denotes the ice-frost point temperature as -40 (1), -55 (2), or -70°C (3) and y denotes the transect as H_2SO_4 (1), NH_4HSO_4 (2), or $(\text{NH}_4)_2\text{SO}_4$ (3). (A) H_2SO_4 temperature transect along the x-axis in Fig. 1. (B) NH_4HSO_4 temperature transect along $m = 1.375$ in Fig. 1. (C) $(\text{NH}_4)_2\text{SO}_4$ temperature transect along the y-axis in Fig. 1.

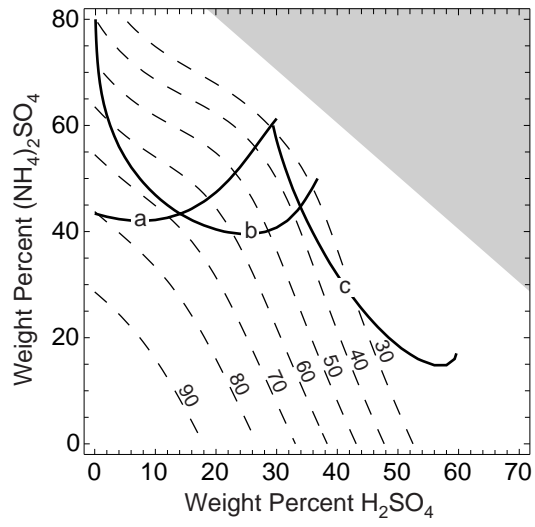
Running Heads

MARTIN: PHASE TRANSFORMATIONS OF $(\text{NH}_4)_2\text{SO}_4\text{-H}_2\text{SO}_4\text{-H}_2\text{O}$

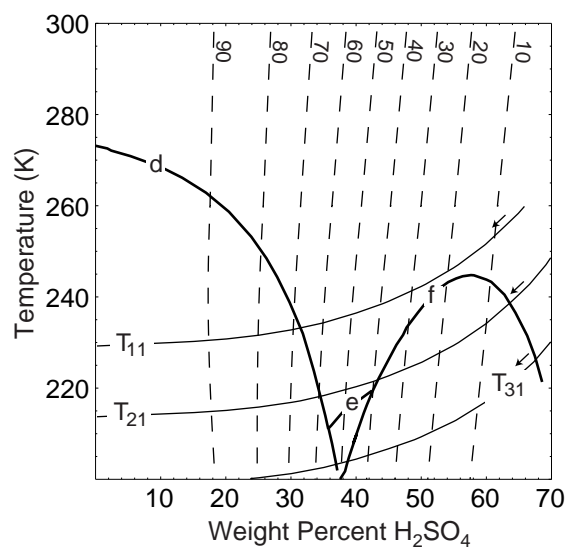
MARTIN: PHASE TRANSFORMATIONS OF $(\text{NH}_4)_2\text{SO}_4\text{-H}_2\text{SO}_4\text{-H}_2\text{O}$

MARTIN: PHASE TRANSFORMATIONS OF $(\text{NH}_4)_2\text{SO}_4\text{-H}_2\text{SO}_4\text{-H}_2\text{O}$

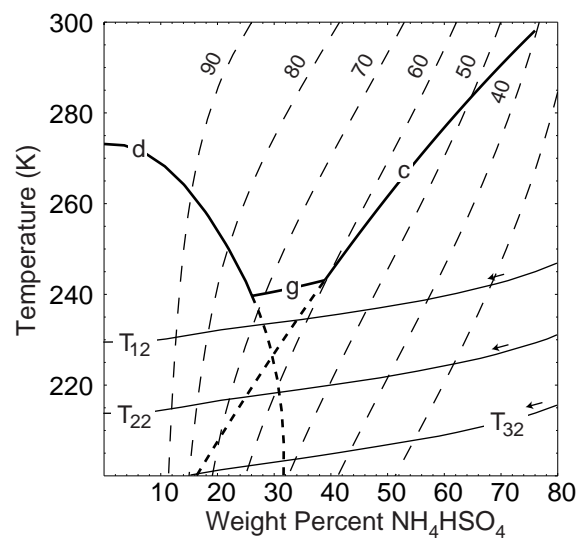
MS# 4166, Scot T. Martin, Figure 1



MS# 4166, Scot T. Martin, Figure 2A



MS# 4166, Scot T. Martin, Figure 2B



MS# 4166, Scot T. Martin, Figure 2C

